DOI: https://doi.org/10.37434/tpwj2025.11.04

FEATURES OF THE STRESSED STATE OF WELDED ABSORBER ELEMENTS IN THE CONTROL AND PROTECTION SYSTEM OF WWER-1000 DURING ASSEMBLY AND SUBSEQUENT OPERATION

O.S. Milenin, O.A. Velykoivanenko, H.P. Rozynka, O.O. Makhnenko

E.O. Paton Electric Welding Institute of the NASU
11 Kazymyr Malevych Str., 03150, Kyiv, Ukraine

ABSTRACT

The control and protection system (CPS) with absorber elements (AE) plays a key role in the stable and safe operation of WWER-1000 reactor, ensuring power regulation and emergency shutdown. The reliability of CPS AE directly depends on the integrity of the AE shell components, which are subjected to both welding stresses during assembly and to operational loads. A critical reliability factor for such structures is the stress-strain state at various stages of assembly and operation. This study focuses on the analysis of the SSS in the AE shell components caused by the technological phase of assembly welding and operational loading. Numerical modeling of thermodeformational processes shows that the geometric characteristics of the structure result in the fundamental difference in the stress distribution: a biaxial stressed state forms in the area where the cone is welded to the AE shell, and a triaxial stressed state develops in the zone where the tip is joined to AE shell. It is shown that during reactor emergency shutdown and cooling to room temperature, there is a significant drop in the external coolant pressure and a sharp increase in the maximum stresses within the AE shell wall, indicating an increased risk of integrity loss.

KEYWORDS: nuclear reactor, WWER-1000, control and protection system, absorber elements, welded shells, stressed state, modeling

INTRODUCTION

Nuclear power plant operation is associated with the need to guarantee a high level of safety of both the individual components, and the entire cycle of energy generation. This concerns ensuring the integrity of the structures and components of nuclear reactors and accompanying process equipment, planned running of the processes of nuclear and related reactions, avoiding the release of radioactive substances into the environment, safety of service engineering personnel, etc. The complexity and interrelation of the physical and technological processes, as well as a considerable influence of the human factor necessitates a detailed and comprehensive study of the regularities of their impact on safe operation of nuclear reactors.

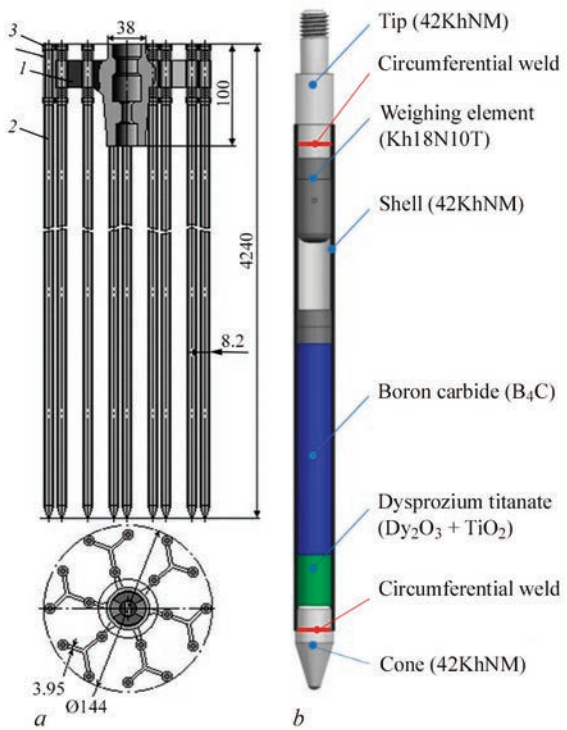

Figure 1. Sketches of CPS absorbing elements AE (*a*) and absorbing rod AR (*b*): *1* — head; *2* — AR; *3* — nut; *4* — spring

An important part of the reactor is the control and protection system (CPS), which includes the absorber elements (CPS AE) (Figure 1, *a*), which have a critical role in ensuring a stable and safe operation of the reactor, fulfilling a range of important functions [1, 2]. First, CPS allows precisely controlling and regulating the reactor power, ensuring its effective and safe operation. It is responsible for starting the reactor and gradual reaching of the specified power level, as well as a change of the reactor operating modes by switching from one power level to another one. Secondly, CPS ensures the possibility of prompt termination of the chain reaction of nuclear fission in the case of emergency situations or the need to quickly reduce the power. This is achieved by dropping the absorbing elements into the AE core, preventing further development of the reaction. Finally, CPS is an important element of general reactor safety, as its functioning

allows eliminating the probability of uncontrolled development of the nuclear reaction, thus preventing the possible emergencies.

Thus, ensuring safe operation of a nuclear reactor is directly related to guaranteeing the integrity of CPS components. The importance of this factor led to formulation of a range of regulatory requirements as to analysis of the technical state and serviceability of individual CPS components, in particular, strength and tightness of absorbing elements (AE) [3–5].

A feature of these AE is their complex profile and presence of assembly welded joints of the shell with the cone and tip. This, in its turn, determines the complex distribution of mechanical stresses under the operation conditions, caused by a nonlinear interaction of residual postweld stresses with the operational stresses. It is known that the magnitude of the stresses characterizes the proneness to brittle, brittle-ductile and fatigue fracture of structural materials [6–8]. Therefore, understanding of the regularities of stress distribution in the cross-section of shell CPS AE at different stages of operation is important for correct prediction of the reliability during design, technical diagnostics of the actual state and extension of the service life for the post-project period.

THE OBJECTIVE

of this study is determination of the influence of the process of assembly welding and thermal-force operational impact on the stress-strain state (SSS) of the shell elements of CPS AE.

AE (Figure 1, *b*) is a rod with a cylindrical shell from chromium-nickel alloy 42KhNM [9] with the outer diameter of 8.2 mm and wall thickness of 0.50–0.55 mm, hermetically sealed with end parts (tip which ensures connection to the CPS AE load-carrying system, and weighing cone) and filled with absorbing material [10].

Temperature dependencies of physical and mechanical properties of corrosion-resistant 42KhNM alloy are given in the Table 1. The yield strength of 42KhNM alloy during manufacture of seamless thin-walled cold-deformed pipes is specified at the level of σ_Y = 520 MPa at T = 20 °C, σ_Y = 245 MPa at T = 375 °C.

The shell sealing is performed by electric arc welding of the upper and lower end parts in inert gas atmosphere. Located inside the shell is an absorber element from a dispersion material, such as boron carbide (B_4C) and dysprosium titanate (Dy_2O_3 + TiO_2) in an aluminium matrix or hafnium [11]. Depletion of these elements and their swelling leads to development of excess internal pressure P_{int} inside the cylindrical shell (close to 3.0 MPa) and under certain

Table 1. Temperature dependencies of physical and mechanical properties of 42KhNM alloy [9]

T, °C	E, GPa	$\alpha \cdot 10^6$, 1/°C	λ, W/(cm·°C)	$c\rho$, J/(cm^3·°C)
20	234	14.5	0.050	3.550
100	223	15.0	0.100	3.686
200	218	15.6	0.130	3.800
300	210	16.0	0.150	3.854
400	204	16.6	0.180	3.955
500	196	17.0	0.205	3.991
600	188	17.5	0.230	4.040
700	143	18.0	0.230	4.043
800	135	18.5	0.230	4.113
900	118	19.0	0.230	4.115
1000	96	19.5	0.230	4.115
1100	46	19.5	0.230	4.115
1200	8	19.5	0.230	4.115

conditions it affects the load-carrying capacity and quantitative indices of the technical state. According to the design conditions of AE operation, there is the external pressure of the coolant P_{ex} = 16 MPa at the temperature of T_0 = 350 °C. In addition to the design mode, it is also necessary to take into account the situation of emergency shutdown of the reactor, when P_{ex} drops to zero, and the temperature decreases to room temperature, T_0 = 20 °C. Summing up the above-said, we can single out three characteristic states of CPS AE, namely: after assembly welding, under the conditions of design operation in the stationary mode and in case of reactor shut-down and its cooling.

As was noted above, a typical characteristic of reliability of critical elements of power-generating equipment, which is determined during assessment of the reactor condition, is the level of mechanical stresses, formed at different stages of operation. For the case of shell CPS AE stress distribution in the structure cross-section is determined by interaction of postweld stresses with external loading and temperature influence. Therefore, in order to predict the stress fields, it is necessary to take into account both the technological aspect of assembly welding, i.e. kinetics of the thermodeformational state of the structure material under the impact of the local heat source down to complete cooling and reaching the residual state, and further heating and loading during operation.

Spatial heterogeneity and nonlinear kinetics of the physical and mechanical processes, which determine the current and residual SSS of the structure during assembly welding and further operation, complicates the use of simplified analytical methods of analysis. More over, small scale of CPS AE components and their geometric shape make the use of instrumental NDT methods more complicated. Therefore, it is expedient to apply the methods of mathematical

modeling and computer simulation of the respective technological processes based on multiphysical mathematical models and finite element means of their numerical implementation.

In this paper the problem of numerical prediction of the temperature field kinetics and development of elastoplastic deformations was considered within the framework of formulation of the boundary problem of nonstationary thermoplasticity. The temperature field kinetics was described by numerical solution of the nonstationary heat-conductivity equation, namely [12]:

$$c\rho(r,\beta,z,T)\frac{\partial T(r,\beta,z)}{\partial \tau} = \nabla\left[\lambda(r,\beta,z,T)\nabla T(r,\beta,z)\right], \quad (1)$$

where λ, $c\rho$ is the heat conductivity and volumetric heat capacity of the structure material in this point, respectively, as a function of spatial coordinates and temperature.

The heat source is the Gaussian surface heat flux from the welding arc into the area of the assembly joint of the tip with the shell and of the cone with the shell. Heat dissipation through the surface in welding occurs due to Newton–Richmann's (convective heat transfer) and Stefan–Boltzmann laws (infrared radiation), and it is described by the respective heat flows. Thus, the boundary conditions as to the formulated problem (1) are as follows [12]:

$$-\lambda(T)\frac{\partial T}{\partial n} = -q_W + \alpha_T(T - T_C) + \varepsilon\sigma_{SB}\left(T^4 - T_C^4\right), \quad (2)$$

where n is the normal to the surface; a_T is the heat transfer coefficient; T_C is the ambient temperature; ε is surface emissivity; σ_{SB} is the Stephan-Boltzmann constant; q_W is the welding heat energy flow.

Mathematical consideration of the unified problem of the kinetics of the temperature field and SSS development is based on the finite element description, using eight-node finite elements (FE). Within the FE volume, the distributions of temperatures, stresses and strains are taken to be homogeneous, and the increment of the strain tensor can be represented according to the following expression [13]:

$$d\varepsilon_{ij} = d\varepsilon_{ij}^e + d\varepsilon_{ij}^p + \delta_{ij}d\varepsilon_T, \quad (3)$$

where $d\varepsilon_{ij}^e, d\varepsilon_{ij}^p, \delta_{ij}\cdot d\varepsilon_T$ are the components of strain tensor increment, due to the elastic mechanism of deformation, instantaneous plasticity strains and kinetics of a heterogeneous temperature field, respectively.

Tensors of mechanical stresses σ_{ij} and elastic strains $d\varepsilon_{ij}^e$ are related to each other by the generalized Hooke's law, i.e. [14]:

$$\varepsilon_{ij}^e = \frac{\sigma_{ij} - \delta_{ij}\sigma}{2G} + \delta_{ij}(K\sigma + \varphi), \quad (4)$$

where σ is the mean value of normal components of stress tensor σ_{ij}, i.e. $\sigma = \frac{(\sigma_{\beta\beta} + \sigma_{zz} + \sigma_{rr})}{3}$, $K = \frac{1-2\nu}{E}$ is the bulk modulus, G is the shear modulus.

Increment of instantaneous plasticity strain $d\varepsilon_{ij}^p$ from the stressed state in a specific FE can be calculated using a linear dependence of scalar function Λ and deviator component of the stress tensor, namely [14]:

$$d\varepsilon_{ij}^p = d\Lambda(\sigma_{ij} - \delta_{ij}\sigma). \quad (5)$$

Specific value of function Λ depends on the stressed state in the considered area of the structure, as well as on the shape of the material yield surface, which is characterized by stresses σ_x:

$$d\Lambda = 0, \text{ if } \sigma_i < \sigma_s,$$
$$d\Lambda > 0, \text{ if } \sigma_i = \sigma_s,$$
$$\text{state } \sigma_i > \sigma_s \text{ is inadmissible.} \quad (6)$$

Proceeding from the above, the increments of the strain tensor can be represented in the form of superposition of the increment of the respective components:

$$\Delta\varepsilon_{ij} = \Psi\left(\sigma_{ij} - \delta_{ij}\sigma\right) + \delta_{ij}\left(K\sigma + \Delta\varepsilon_T\right) - \frac{1}{2G}\left(\sigma_{ij} - \delta_{ij}\sigma\right)^* - \left(K\sigma\right)^*, \quad (7)$$

where symbol "*" refers the respective variable to the previous tracking step; Ψ is the function of the material state, which determines the condition of plastic flow of the material according to von Mises criterion [15]:

$$\Psi = \frac{1}{2G}, \text{ if } \sigma_i < \sigma_s = \sigma_Y,$$
$$\Psi > \frac{1}{2G}, \text{ if } \sigma_i = \sigma_s,$$
$$\text{state } \sigma_i > \sigma_s \text{ is inadmissible.} \quad (8)$$

Function Ψ is determined by iteration at each step of digital tracing within the boundary problem of nonstationary thermoplasticity, which allows solving the nonlinearity by the plastic yield of the material.

Computer implementation of the given algorithms allowed performing analysis of the regularity of

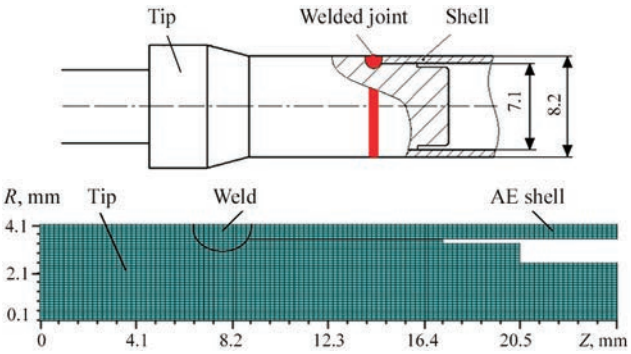

Figure 2. Sketch and finite element model of a welded joint of CPS AE shell with a tip [10]

formation of CPS AE SSS at the stage of assembly welding and further operation. Welding the tip to the shell (Figure 2) in an argon atmosphere is performed in the following mode according to [10]: U = 120 V; I = 20 A; v_w = 13 m/h. Welding of the assembled cone to the shell (Figure 3) in an argon atmosphere occurs in the following mode: U = 10 V; I = 30 A; v_w = 12 m/h.

As shown by the calculation results (Figure 4, *a*), the shape of penetration in the area of joining the cone to the shell of the AE ensures a proper permanent joint of these components. Residual postweld stresses are characterized by an increase in the normal stresses in the circumferential ($\sigma_{\beta\beta} \approx 590$ MPa) and axial ($\sigma_{zz} \approx 540$ MPa) directions in the area close to the middle of the cone wall thickness (Figure 5). In addition, the zone of tensile stresses extends right up to the internal surface of the shell in the area of the joint with the cone. Contrarily, the external surface is characterized by compressive normal stresses. The maximum values of circumferential stresses are close to those of the material yield strength, according to von Mises plasticity criterion. In contrast to this, the radial component of stress is almost five times lower ($\sigma_{rr} \approx 105$ MPa). Such a biaxiality of the stress field, in general, is characteristic for the cylindrical shell el-

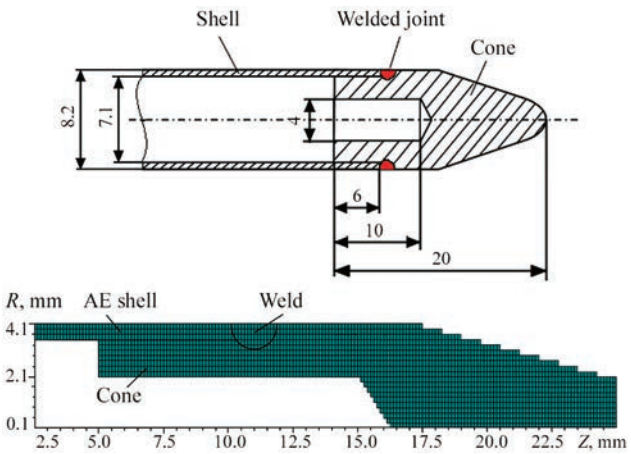

Figure 3. Sketch and finite element model of a welded joint of the CPS AE shell with the cone [10]

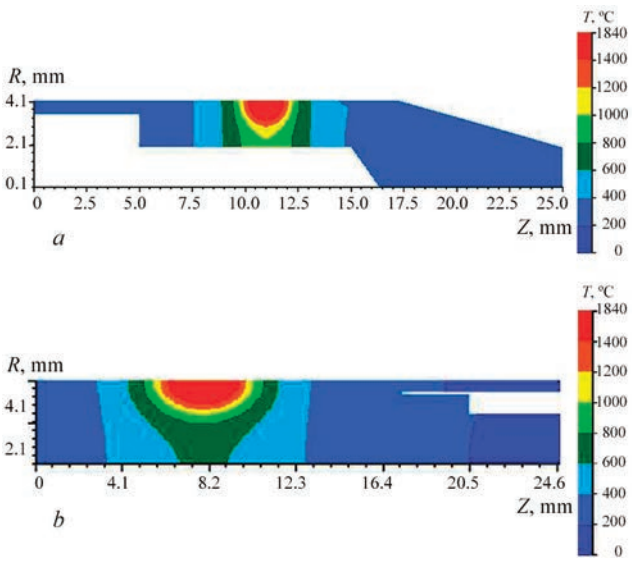

Figure 4. Calculated distribution of maximum temperatures in the zone of the welded joint of CPS AE shell with the cone (*a*) and with the tip (*b*)

ements, joined by a circumferential weld, while the features of stress distribution are due to the ratio of the wall thickness to the cylinder radius.

Under operating load conditions according to the design stationary mode (T_0 = 350 °C, P_{ex} = 16 MPa, P_{int} = 3 MPa) the stress distribution does not change in principle (Figure 6). However, a certain reduction of maximum stresses ($\sigma_{\beta\beta} \approx 500$ MPa, $\sigma_{zz} \approx 470$ MPa, $\sigma_{rr} \approx 85$ MPa) is observed, caused by the natural lowering of the yield strength at the temperature of

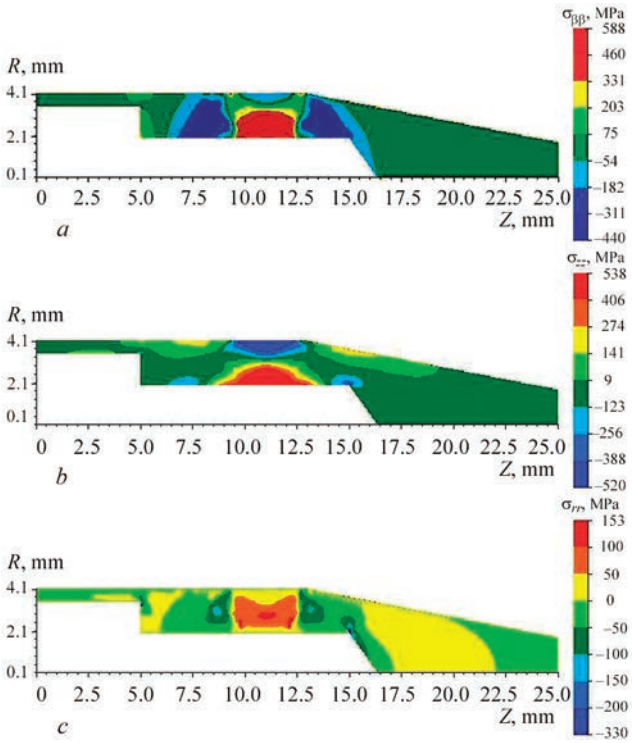

Figure 5. Calculated distributions of residual postweld stresses in the zone of the welded joint of the cone with CPS AE shell: *a* — circumferential component; *b* — axial component; *c* — radial component

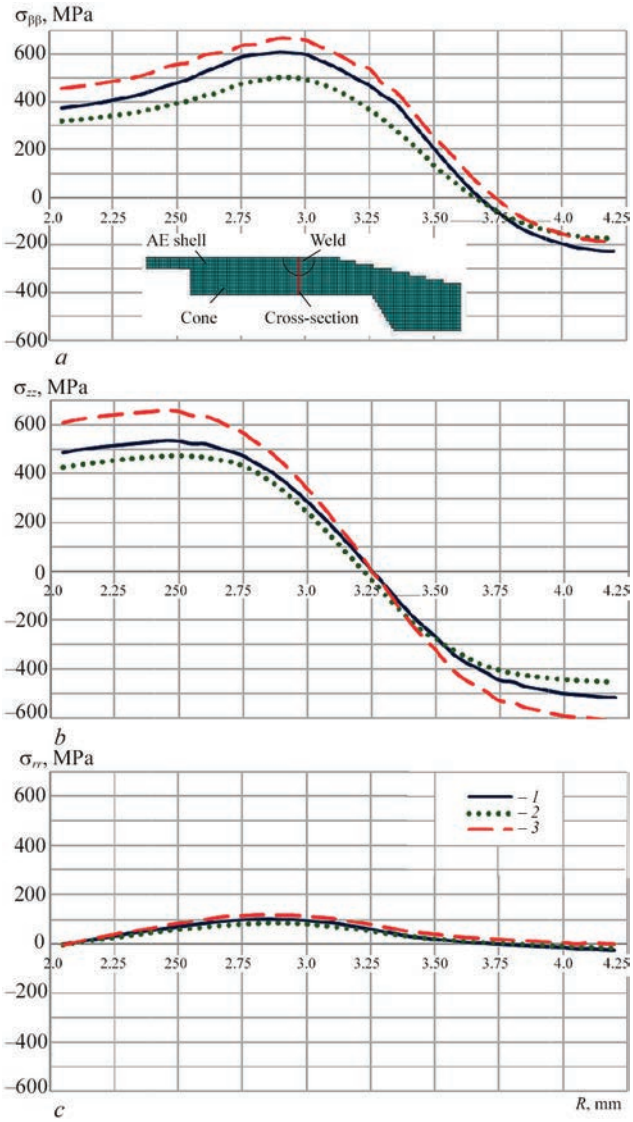

Figure 6. Calculated distributions of residual and operational stresses in the cross-section of the welded joint of the cone with the AE shell; circumferential (*a*), axial (*b*), radial (*c*): *1* — residual stresses; *2* — T_0 = 350 °C, P_{int} = 3 MPa, P_{ext} = 16 MPa; *3* — T_0 = 20 °C, P_{int} = 3 MPa

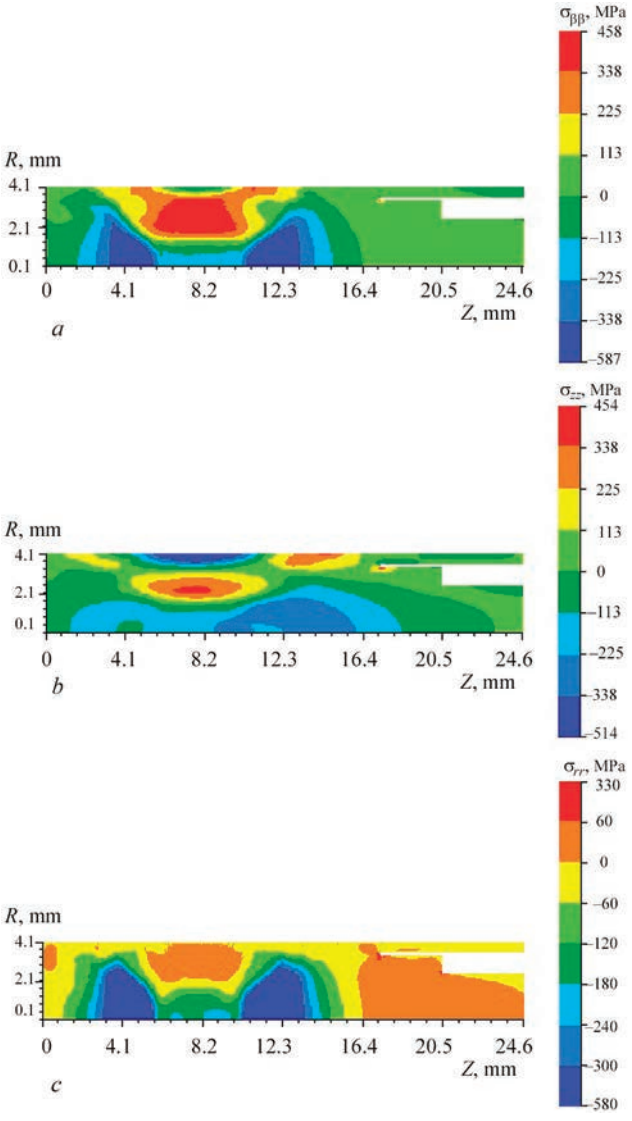

Figure 7. Calculated distributions of residual postweld stresses in the zone of the welded joint of the tip with the CPS AE shell: circumferential (*a*), axial (*b*) radial (*c*)

350 °C, compared to room temperature, at which the process of assembly welding was conducted. The operational situation of reactor shutdown, CPS AE cooling to room temperature and lowering of external pressure (P_{int} = 3 MPa, P_{ext} = 0 MPa, T_0 = 20 °C) leads to a significant increase of maximum stresses ($\sigma_{\beta\beta} \approx 670$ MPa, $\sigma_{zz} \approx 660$ MPa, $\sigma_{rr} \approx 120$ MPa) in the shell wall (Figure 6) for the reason that the internal pressure from the filler is not compensated by the external pressure of the coolant, so that it can be considered as the most unfavourable in terms of strength of the welded joint of AE shell with the cone.

Distribution of maximum temperatures in the area of joining the tip to the shell demonstrates significant penetration, which ensures a proper permanent joint of individual parts (Figure 4, *b*). A fundamental difference in the residual stress distribution (Figure 7) is the fact that the welded joint is located in the CPS AE solid part, so that the area of high postweld circumferential and axial stresses forms in the subsurface zone, where maximum lowering of the joint strength is to be expected. In addition, compared to the welded joint of the shell with the cone a lower level of maximum residual stresses is observed ($\sigma_{\beta\beta} \approx 460$ MPa, $\sigma_{zz} \approx 350$ MPa, $\sigma_{rr} \approx 35$ MPa).

Similar to the case of the area of the joint of the cone with the shell, under the conditions of design operation a certain lowering of stresses ($\sigma_{\beta\beta} \approx 420$ MPa, $\sigma_{zz} \approx 300$ MPa, $\sigma_{rr} \approx 10$ MPa) is observed in the area of the joint of the tip with the shell (Figure 8), while the most hazardous stressed state develops during reactor shutdown (Figure 8), when there are no compensating compressive forces from external pressure, while redistribution of stresses with increase of the yield strength as a result of temperature lowering from 350 °C to room temperature causes an increase of nor-

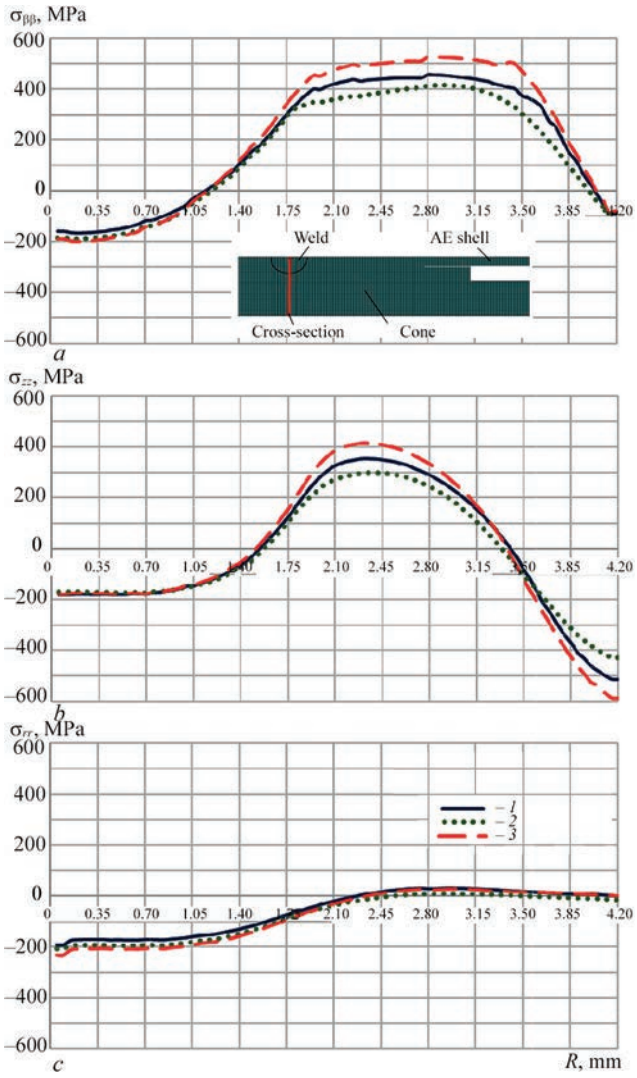

Figure 8. Calculated distributions of residual and operational stresses in the cross-section of a welded joint of the AE tip with the shell: circumferential (*a*), axial (*b*), radial (*c*): *1* — residual stresses; *2* — T_0 = 350 °C, P_{int} = 3 MPa, P_{ext} = 16 MPa; *3* — T_0 = 20 °C, P_{int} = 3 MPa

mal stresses by more than 100 MPa ($\sigma_{\beta\beta} \approx 530$ MPa) $\sigma_{zz} \approx 410$ MPa, $\sigma_{rr} \approx 30$ MPa).

CONCLUSIONS

1. A model was developed of the kinetics of the temperature field and stress-strain state of CPS AE of WWER-1000 during assembly welding of the cone to the AE shell and of the tip to the AE shell was developed. Used for this purpose, was a numerical solution of a nonstationary equation of heat conductivity alongside with successive tracking of the development of elastoplastic strains of a continuous medium by finite element solution of the boundary problem of nonstationary thermoplasticity.

2. It is shown that development of a thermodeformational state of CPS AE structure during welding of the cone to the shell leads to formation of a biaxial SSS, characteristic for welding thick-walled pipes, with considerable prevalence of circumferential and longitudinal stresses. In the zone of connection of the CPS AE tip to the shell, the weld is located in the solid part of the structure which leads to formation of a subsurface area of intensive postweld circumferential and axial stresses. The maximum radial stresses rise to the level of other components of the stress tensor. As a result, this area of the structure is in the state of triaxial stress.

3. During operation, the total pattern of stress distribution is preserved, but their maximum values become lower. This phenomenon is related to the fact that at the working temperature of 350 °C the material yield strength decreases, compared to its room temperature value, at which assembly welding was performed. As a result, the material becomes more susceptible to plastic strains, which promotes partial redistribution of stresses.

4. During the reactor shutdown and its cooling to room temperature a significant lowering of the external pressure takes place. As the internal pressure of the filler is no longer balanced by the coolant pressure, it causes an abrupt increase of maximum stresses in the wall of CPS AE shell. Such a situation creates the most unfavourable conditions for strength of welded joints, increasing the risk of defect development and deterioration of the operational reliability of the structure.

REFERENCES

1. Misak, J. (2024) History, specific design features, and evolution of WWER reactors. *Nuclear Power Reactor Designs: From History to Advances*, **2024**, 57–91. DOI: https://doi.org/10.1016/B978-0-323-99880-2.00004-7
2. Pyrohov, T., Korolev, A., Inyushev, V., Kurov, V. (2020) Analysis of accidents of the WWER-1000 reactor in which emergency cooling heat exchangers operate. *Technology Audit and Production Reserves*, 5(**55**), 43–47. DOI: https://doi.org/10.15587/2706-5448.2020.213227
3. (2013) *Guidelines for integrity and lifetime assessment of components and piping in WWER nuclear power plants* (VERLIFE). Vienna, Int. At. Energy Agency.
4. PNAE G-7-002–86: *Standards for strength calculation of equipment and pipelines of nuclear power installations* [in Ukrainian].
5. (2016) API 579-1/ASME FFS-1: Fitness-For-Service. Washington, American Petroleum Institute, American Society of Mechanical Engineers.
6. Lemaitre, J., Desmorat, R. (2005) *Engineering damage mechanics. Ductile, creep, fatigue and brittle failures*. Berlin, Springer-Verlag.
7. Amsterdam, E., Grooteman, F. (2016) The influence of stress state on the exponent in the power law equation of fatigue crack growth. *Inter. J. Fatigue*, 82(**3**), 572–578. DOI: https://doi.org/10.1016/j.ijfatigue.2015.09.013
8. Dormieux, L., Kondo, D. (2016) *Micromechanics of fracture and damage*. Vol. 1. London: ISTE Ltd.
9. (1967) *Physical properties of steels and alloys used in power engineering:* Refer. Book. Ed. by B.E. Neimark. Moscow, Energiya [in Russian].
10. Kushtym, A.V., Zihunov, V.V., Hrytsyna, V.M. et al. (2023) Characteristics of welded joints of absorbing elements from

42KhNM alloy for control and protection system rods of WWER-1000. *Yaderna ta Radiatsiina Bezpeka*, 4(**100**), 38–48 DOI: https://doi.org/10.32918/nrs.2023.4(100).04 [in Ukrainian].
11. Risovani, V.D., Zakharov, A.Z., Muraleva, E.M. et al. (2019) Dysprosium hafnate as absorbing material for control rods. *J. of Nuclear Materials*, 355(**1–3**), 163–170. DOI: https://doi.org/10.1016/j.jnucmat.2006.05.029
12. Karkhin, V.A. (2019) *Thermal processes in welding*. Singapore, Springer Singapore.
13. Velikoivanenko, E.A., Milenin, A.S., Rozynka, G.F. et al. (2019) Prediction of susceptibility of welded joints of titan γ-aluminide based alloy to cold cracking in electron-beam welding. *Tekhnologicheskie Sistemy*, **3**, 73–80. DOI: https://dx.doi.org/10.29010/88.9
14. Velikoivanenko, E.A., Milenin, A.S., Popov, A.V. et al. (2019) Methods of numerical forecasting of the working performance of welded structures on computers of hybrid architecture. *Cybernetics and Systems Analysis,* 55(**1**), 117–127. DOI: https://doi.org/10.1007/s10559-019-00117-8
15. Makhnenko, V.I. (2006) *Safe operation resource of welded joints and assemblies of modern structures. Kyiv*, Naukova Dumka [in Russian].

ORCID
O.S. Milenin: 0000-0002-9465-7710,
O.A. Velykoivanenko: 0009-0007-3704-2000,
H.P. Rozynka: 0009-0009-1750-7266,
O.O. Makhnenko: 0000-0003-2319-2976

CONFLICT OF INTEREST
The Authors declare no conflict of interest

CORRESPONDING AUTHOR
O.S. Milenin
E.O. Paton Electric Welding Institute of the NASU
11 Kazymyr Malevych Str., 03150, Kyiv, Ukraine.
E-mail: asmilenin@ukr.net

SUGGESTED CITATION
O.S. Milenin, O.A. Velykoivanenko, H.P. Rozynka, O.O. Makhnenko (2025) Features of the stressed state of welded absorber elements in the control and protection system of WWER-1000 during assembly and subsequent operation.
The Paton Welding J., **11**, 28–34.
DOI: https://doi.org/10.37434/tpwj2025.11.04

JOURNAL HOME PAGE
https://patonpublishinghouse.com/eng/journals/tpwj

Received: 10.06.2025
Received in revised form: 24.07.2025
Accepted: 19.11.202